Ultrasonics Sonochemistry 28 (2016) 31–38

Contents lists available at ScienceDirect

Ultrasonics Sonochemistry

journal homepage: www.elsevier.com/locate/ultson

Ultrasound mediated destruction of multifunctional microbubbles for image guided delivery of oxygen and drugs

Shufang Chang [a,b,1], Ting Si [a,c,1], Shiwu Zhang [a,c], Mark A. Merrick [d], David E. Cohn [e], Ronald X. Xu [a,c,*]

[a] Department of Biomedical Engineering, The Ohio State University, Columbus, OH 43210, USA
[b] Department of Obstetrics and Gynecology, Second Affiliated Hospital of Chongqing Medical University, Chongqing 400010, China
[c] College of Engineering, University of Science and Technology of China, Hefei, Anhui 230027, China
[d] Division of Health & Rehabilitation Sciences, The Ohio State University Medical Center, Columbus, OH 43210, USA
[e] Department of Obstetrics and Gynecology, The Ohio State University Medical Center, Columbus, OH 43210, USA

ARTICLE INFO

Article history:
Received 6 January 2015
Received in revised form 18 May 2015
Accepted 24 June 2015
Available online 25 June 2015

Keywords:
Oxygen
Perfluorocarbon
Multifunctional microbubbles
Fluorescence imaging
Ultrasound targeted microbubble destruction
Drug delivery

ABSTRACT

We synthesized multifunctional activatible microbubbles (MAMs) for ultrasound mediated delivery of oxygen and drugs with both ultrasound and fluorescence imaging guidance. Oxygen enriched perfluorocarbon (PFC) compound was encapsulated in liposome microbubbles (MBs) by a modified emulsification process. DiI dye was loaded as a model drug. The ultrasound targeted microbubble destruction (UTMD) process was guided by both ultrasonography and fluorescence imaging modalities. The process was validated in both a dialysis membrane tube model and a porcine carotid artery model. Our experiment results show that the UTMD process effectively facilitates the controlled delivery of oxygen and drug at the disease site and that the MAM agent enables ultrasound and fluorescence imaging guidance of the UTMD process. The proposed MAM agent can be potentially used for UTMD-mediated combination therapy in hypoxic ovarian cancer.

1. Introduction

Ovarian cancer is the ninth most common cancer and ranks fifth as the cause of cancer death in women [1]. Patients commonly develop ovarian cancer asymptomatically and present with peritoneal metastasis at the time of diagnosis. Since most often the disease has spread from the ovaries at presentation, the overall outcome is poor, with less than 30% survival in 5 years [2]. Currently, the standard first-line therapy for advanced ovarian cancer includes surgical staging or cytoreductive surgery, followed by intravenous (i.v.) or intraperitoneal (i.p.) chemotherapy with paclitaxel (PTX) and carboplatin administered every three weeks. However, 80% of patients will relapse the treatment and ultimately develop the resistant disease [3]. The development of drug resistance in ovarian cancer is closely associated with tumor hypoxia [4]. Hypoxia comprises therapeutic effectiveness of many anticancer drugs through multiple mechanisms such as increased acidity, increased hypoxia-induced factor 1α (HIF-1α), generation of free radicals, and cellular adaptation [5–7]. Therefore, hyperoxic treatments, such as oxygen respiration and hyperbaric chamber, are commonly prescribed before radiotherapy or chemotherapy in order to boost tumor oxygenation, improve drug uptake, and enhance tumor response [8–10]. However, these systemic treatment options have limited specificity and efficacy.

The emergence of the microbubbles (MBs) and the ultrasound targeted microbubble destruction (UTMD) technique offers a new opportunity for delivering oxygen and anti-cancer drugs to the hypoxic tumor site simultaneously in order to overcome the hypoxia-induced chemoresistance. Originally used as a contrast enhancement agent in ultrasonography, MBs have attracted more and more research interests as a disease-targeting agent for molecular imaging [11,12] and as a biocompatible carrier for drug delivery [13]. We have encapsulated perflourocarbon compounds (PFC) in liposome MBs and loaded the MBs with paclitaxel (PTX) for UTMD-mediated drug delivery. Our previous in vitro and in vivo studies have demonstrated that the UTMD process can effectively enhance the PTX deposition at the disease site and improve the therapeutic outcome [14,15]. We have also delivered oxygen and PTX simultaneously for combination therapy in hypoxic ovarian

Abbreviation: MAMs, multifunctional activatible microbubbles.

* Corresponding author at: 270 Bevis Hall, Columbus, OH 43210, USA.
E-mail address: xu.ronald@gmail.com (R.X. Xu).

[1] These authors contributed equally to this work.

http://dx.doi.org/10.1016/j.ultsonch.2015.06.024
1350-4177/

cancer cells. Our in vitro study showed that simultaneous delivery of oxygen and PTX significantly enhanced the local oxygen release, the anti-proliferative activities, and the cell apoptosis ratio for hypoxic ovarian cancer cells, superior to other treatment groups such as applying PTX only or applying PTX-loaded microbubbles with or without ultrasound mediation (unpublished data). Our in vivo study in ovarian cancer xenograft mice showed that intravenous injection of oxygen and PTX-loaded MBs followed by UTMD yielded the increased tumor apoptosis, the reduced VEGF expression, the decreased expressions of HIF-1α and P-gp, and the significant inhibition of tumor growth [16]. These studies suggest that the oxygen and PTX-loaded MBs and the UTMD process may provide a promising drug delivery strategy for the combination treatment of hypoxic ovarian cancer. These studies also suggest the need of quantitative imaging techniques for reliable control of the UTMD-mediated drug delivery process. Currently, the UTMD process is commonly guided by ultrasonography. However, the imaging sensitivity and specificity of ultrasonography is sub-optimal owing to hyperechoic artifacts and non-specific gas bubbles. We have encapsulated fluorescence agents in MBs for potential use of fluorescence imaging guided drug delivery [17,18]. Considering the high molecular sensitivity of fluorescence imaging and the deep imaging depth of ultrasonography, it is rationale to load oxygen, anti-cancer drugs, and fluorescence dyes in liposome MBs so that the UTMD-mediated drug delivery process can be guided by both ultrasonography and fluorescence imaging modalities simultaneously.

In this paper, we demonstrated simultaneous delivery of oxygen and therapeutics by an image-guided UTMD process. To simplify the experiment design, a commonly used fluorescence dye, [1,1′-Dioctadecyl-3,3,3′,3′-tetramethylindocarbocyanine iodide] (DiI), was used as the model drug. To minimize the unnecessary use of the lab animals, we validated the image-guided UTMD process in a benchtop phantom and an ex vivo tissue model.

2. Materials and methods

2.1. Materials

Hydrogenated L-α-phosphatidylcholine, polyethylene glycol 40 (PEG-40) stearate, glycerol, Pluronic® F-68 (F68), [4′,6-Diamidino-2-Phenylindole] (DAPI) and propane-1,3-diol were obtained from Sigma–Aldrich Co. Ltd (St. Louis, MO, USA). Methylene chloride (CH_2Cl_2), [1,1′-Dioctadecyl-3,3,3′,3′-tetramethylindocarbocyanine iodide] (DiI) and dimethyl sulfoxide (DMSO) were obtained from Fisher Scientific (Fairlawn, NJ USA). 1,1,1,2,3,4,4,5,5,5-decafluoropentane (a PFC compound with boiling point of 55 °C) was obtained from Fluka (St. Louis, MO, USA). Sodium hydrosulfite was obtained from ACROS (New Jersey, USA).

2.2. Synthesis of oxygen and DiI loaded MAMs

Oxygen and DiI loaded MAMs comprising a PFC core and a lipid shell were fabricated by a modified emulsification process [19], as illustrated in Fig. 1. The lipid suspension was prepared in advance by mixing 50 mg hydrogenated L-α-phosphatidylcholine, 14 mg PEG-40 stearate, 1 ml glycerol (density 1.25 g ml^{-1}), 5 ml propane-1,3-diol (density 1.053 g ml^{-1}), and 50 ml distilled water (mass ratio 1:0.28:25:105:1000) in a conical flask. The mixture was placed in a 42 °C water bath, gently stirred for 30 min, and then cooled down to room temperature. After 100 μl DiI (1 mg/ml) was added to the 18 ml lipid mixture with gentle stirring, the lipid suspension was bubbled with oxygen for 5 min in the dark. After that, 2 ml PFC was bubbled with oxygen gas till saturation and added to DiI lipid suspension. The mixture was homogenized in the dark by an Omni Sonic Ruptor 250 ultrasonic homogenizer (Omni international, Waterbury, CT) at 50 W for 200 s. The above mixture was then added to 20 ml F68 solution (2% w/v) and emulsified in the dark for one minute. The obtained emulsion was centrifuged by Centrifuge 5810R (Eppendorf, Hamburg, Germany) at 800 rpm for 5 min. After centrifugation, the supernatant was discarded and the precipitate was re-dispersed in 40 ml distilled water enriched with oxygen for further use.

The number of the MAMs was counted by a hemacytometer. The MAM concentration was calculated by the following formula: microbubble concentration per milliliter = total microbubble count in 5 squares/80 × 400 × 10^4 × dilution factor. The size distribution and zeta potential were determined by a 90Plus Particle Size Analyzer (Brookhaven Instruments, Holtsville, NY, USA). The MAMs were diluted 100-fold with double-distilled water for size and surface charge measurements. Triplicated measurements were made by averaging 6 data points per sample for three independent samples. The encapsulation efficiency of DiI in MAMs were evaluated by an USB4000-FL fluorescence spectrometer (Ocean Optics Inc., Dunedin, FL, USA) at an excitation wavelength of 550 nm and an emission wavelength of 571 nm. To characterize the encapsulation efficiency, a calibration curve was first obtained by measuring fluorescence intensities at various DiI concentrations. After that, 1 ml DiI loaded MAMs were dissolved in 4 ml DMSO and the fluorescence intensity of the solution was compared with the calibration curve to determine the actual amount of the loaded DiI. The morphology of the DiI loaded activatible MBs was determined by a TCS SL confocal laser scanning microscope (Leica, Heidelberg, Germany) at an excitation wavelength of 543 nm and an emission wavelength of 590 nm.

2.3. Image-guided UTMD process for oxygen delivery

Oxygen and DiI loaded MAMs were fabricated for UTMD-mediated fragmentation and controlled delivery of oxygen. The process was demonstrated in a benchtop setup as sketched in Fig. 2. The setup consists of a Terason 2000 ultrasound imaging system equipped with a 12L5 5–12 MHz linear array probe (Teratech Corp., Burlington, MA, USA), an Omnisound 3000C ultrasound therapy system equipped with a 3 MHz therapeutic ultrasound probe (Physio Technology, Nevada,USA), a 5 MHz immersion focused ultrasound transducer (Olympus NDT Inc., Waltham, MA,USA) connected through a Panametrics 5900PR computer controlled pulse/receiver to a TDS 2024c digital storage oscilloscope (Tektronix, Beaverton, OR, USA), and a plastic tank filled with degassed water. A Spectra/Por dialysis membrane tube (Spectrum Laboratories Inc., Laguna Hills, CA, USA) was mounted at the center of the tank, with both ends connected to an external circulation system (marked as red in Fig. 2). During the experiment, microbubble suspension (concentration: 3 × 10^9 /ml, flow rate: 30 ml/h) was diluted by degassed water (flow rate: 50 ml/h), flowed through the dialysis tube, and collected by a waste collection flask. The therapeutic ultrasound probe was placed five millimeter above the dialysis membrane tube to activate the MAMs at a power density of 1 W/cm^2 and a duty cycle of 20%. A broadband needle hydrophone (ONDA, Sunnyvale, CA, USA) was used to calibrate the transmitted acoustic pressure.

As the ultrasound pulses were applied to the MAMs flowing through the dialysis membrane tube, the dissolved oxygen in the flow and the B-mode image of the tube were acquired by a USB4000 oxygen sensor (Ocean Optics, Dunedin, FL, USA) and the Terason ultrasound probe, respectively. The test results were compared with the control where only degassed water flew through the dialysis membrane tube. Ultrasound mediated fragmentation of the MAMs was also monitored by fluorescence imaging. For this study, the therapeutic ultrasound probe was placed underneath

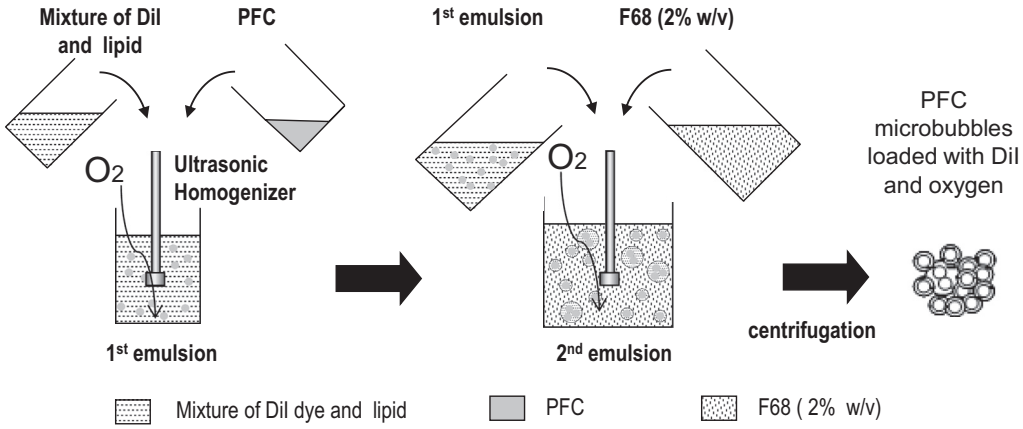

Fig. 1. Microencapsulation process for DiI and oxygen loaded MAMs. The process includes consecutive steps of bubbling lipid and PFC with oxygen gas, mixing DiI dye with lipid, 1st emulsion of lipid with PFC, 2nd emulsion of PFC droplet in water with F68 as surfactant, and final centrifugation.

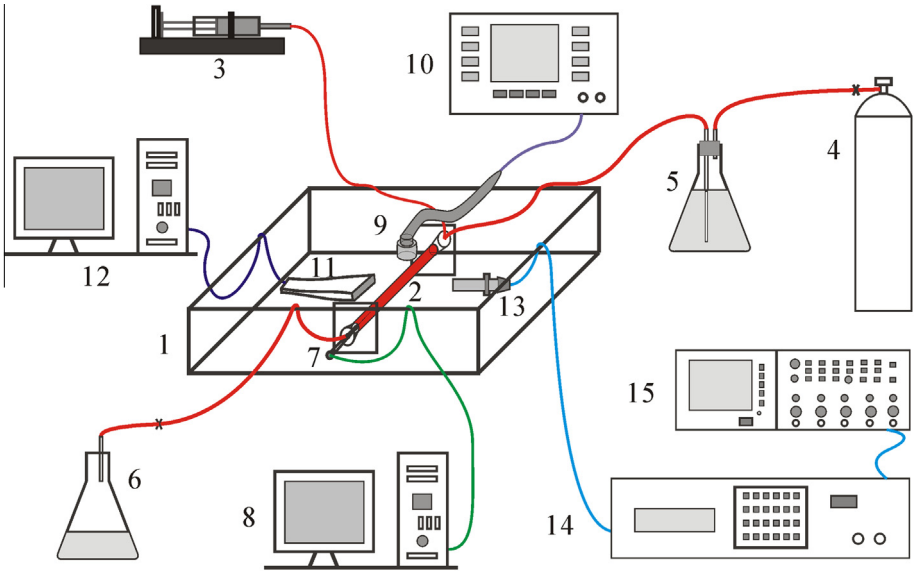

Fig. 2. Schematic of the experimental setup for ultrasound mediated activation of DiI and oxygen loaded MAMs. (1) Water tank filled with degassed water. (2) Dialysis membrane tube. (3) Syringe pump. (4) Nitrogen gas cylinder. (5) Erlenmeyer flask filled with degassed water. (6) Waste collection flask. (7) USB4000 oxygen sensing needle. (8) Computer. (9) 3 MHz therapeutic ultrasound transducer. (10) Omnisound 3000C ultrasound therapy system. (11) Terason 2000 ultrasound imaging probe. (12) Computer. (13) 5 MHz immersion focused ultrasound transducer. (14) 200 MHz pulse/receiver. (15) Digital oscilloscope.

the dialysis membrane tube for MAM fragmentation. The gap between the tube and the ultrasound therapy probe was filled with the ultrasound gel (Parker Laboratories, Inc., Fairfield, NJ, USA). A LabSpec 532 nm DPSS laser system (Laserglow Technologies, Toronto, Ontario, Canada) was connected to a 600 μm multimode optical fiber (Laserglow Technologies, Toronto, Ontario, Canada) to provide uniform illumination in the middle of the tube. An ORCA ER deep cooling NIR CCD camera (Hamamatsu, Bridgewater, NJ) was mounted above the dialysis membrane tube to acquire fluorescence emission, with a FGL550 long pass filter (Thorlabs, Newton, NJ) installed to block the excitation light. As the MAMs flew through the dialysis membrane tube, fluorescence images were continuously acquired before, during, and after the ultrasound pulses were applied. The imaging results were compared with the control where only degassed water flew through the dialysis membrane tube.

2.4. UTMD-mediated drug delivery in a porcine carotid artery model

The use of the MAMs for UTMD mediated drug delivery was demonstrated in a porcine carotid artery model. DiI was used as a model drug to evaluate the delivery efficiency after ultrasound mediation. Common carotid arteries of 3–5 mm in diameter were excised from a fresh swine carcass that had been euthanized after the other procedures approved by The Ohio State University Institutional Animal Care and Use Committee. The arteries were stored in a physiological saline solution (PBS) following the procedure as described in ref. [20]. After the majority of the connective tissue was removed, the carotid artery was tied to plastic connectors on both ends and connected to the microbubble circulation system as shown in Fig. 2, in place of the dialysis membrane tube. The therapeutic ultrasound probe was placed underneath the artery with the gap filled by ultrasound gel. As the MAMs were circulated through the carotid artery, the middle portion of the artery was exposed to 3 MHz therapeutic ultrasound pulses for 5 min at an intensity of 1 W/cm^2 and a duty cycle of 20%. After exposure to ultrasound pulses, the artery was cut along the longitudinal axis and placed flat with its inner side facing up for fluorescence imaging. After fluorescence imaging, serial cross sections (6 μm thick) were obtained at five locations throughout the entire length of the artery and fixed with Tissue-Tek Cryo-OCT compound (Canoga Park, CA, USA) at −80 °C for cryostat section. The frozen

section was stained with DAPI for fluorescence microscopic imaging.

3. Results

3.1. Characterization of DiI and oxygen loaded MAMs

As measured by a particle size analyzer, the average size of the MAMs was 2.65 μm, with a standard deviation of 0.18 μm. The polydispersity index of the MAMs is 6.8%. The core–shell structure of the MAMs is clearly identifiable by confocal and bright field microscopic imaging, as shown in Fig. 3. The DiI loading efficiency was estimated by comparing the emission spectrum of the DiI loaded MAMs with a standard calibration curve (i.e., peak fluorescence emission versus DiI concentration). According to the calibration curve and the fluorescence spectrum in Fig. 4, the DiI concentration in the MAMs was 396 ng/ml. The DiI encapsulation efficiency was 79.2%, as calculated by taking the ratio between the actual amount of the encapsulated DiI and the total amount of DiI dye initially used in the process.

3.2. Acoustic and fluorescence responses of the MAMs

Fig. 5 shows the B-mode ultrasound images of the dialysis membrane tube filled with the MAMs (A) and the DiI dye (B), respectively. The images were acquired under the following experimental conditions: (1) before the therapeutic ultrasound pulses were applied, (2) during the application of the therapeutic ultrasound pulses, (3) after the therapeutic ultrasound pulses were terminated. In these images, the hyperechoic upper and lower walls are ultrasonically visible. Before activation by therapeutic ultrasound pulses, the MAMs (1A) and the DiI dye (1B) show negligible echogenicity. Upon application of 3 MHz therapeutic ultrasound pulses at an intensity of 1 W/cm^2 and a duty cycle of 20%, the MBs vaporize and increase the echogenicity significantly (2A). In comparison, no significant echogenic change is observed for the DiI dye upon exposure to ultrasound pulses (2B). The vertical hyperechoic patterns in (2A) and (2B) are interferential artifacts caused by the therapeutic ultrasound pulses. After the therapeutic ultrasound pulses are terminated, the interferential acoustic artifacts disappear (3A and 3B). The MAM-filled tube shows a consistent echogenic region at the top position, indicating gas bubble formation due to vaporization (3A). In comparison, the DiI dye filled tube resumes to the original acoustic contrast without any echogenic changes (3B). Our experimental results indicate that

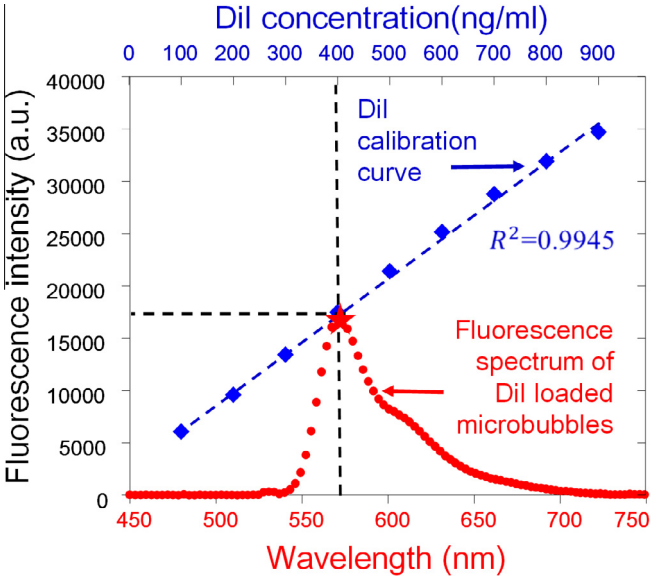

Fig. 4. The fluorescence emission spectrum of DiI loaded MAMs (red dots) in comparison with the DiI calibration curve (blue square). In the standard calibration curve, the peak fluorescence emission is linearly correlated with the DiI concentration (correlation coefficient: 0.9945). In the fluorescence emission spectrum, the fluorescence intensity peaks at the excitation wavelength of 571 nm. The corresponding DiI concentration is 396 ng/ml at this wavelength. Further calculation shows that the DiI loaded MAMs yield an encapsulation efficiency of 79.2%. (For interpretation of the references to colour in this figure caption, the reader is referred to the web version of this article.)

the increased echogenicity of the MAMs after the application of the therapeutic ultrasound pulses is specifically associated with the PFC phase transition and is consistently identifiable by clinical ultrasonography.

Fig. 6 shows the fluorescence images of the dialysis membrane tube filled with the MAMs (A) and the DiI dye (B), respectively. The images were acquired under the following experimental conditions: (1) before the therapeutic ultrasound pulses were applied, (2) during the application of the therapeutic ultrasound pulses, (3) immediately after the therapeutic ultrasound pulses were terminated. Before exposure to therapeutic ultrasound pulses, the MAMs show a greater area of fluorescence emission than that of the DiI dye (Fig. 6, 1A vs. 1B), indicating the multi-scattering effect of the PFC-encapsulating droplets and the enhanced photon migration in the turbid media. Upon exposure to therapeutic ultrasound

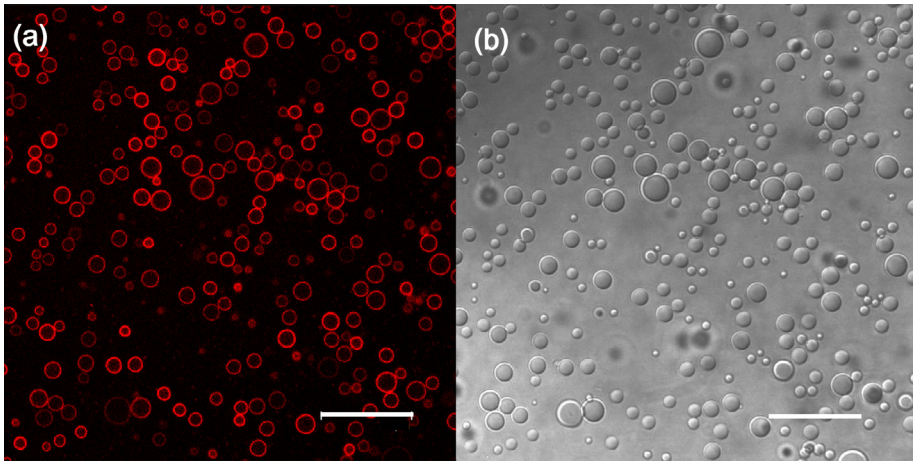

Fig. 3. (a) Confocal fluorescence microscopic image of DiI and oxygen encapsulated MAMs. (b) The corresponding bright field microscopic image. Scale bar: 15 μm.

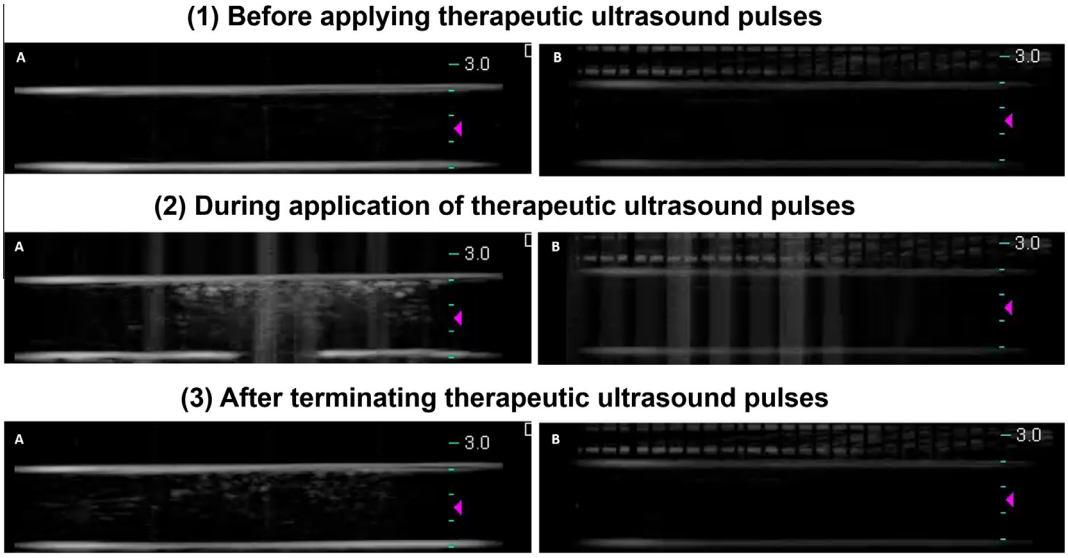

Fig. 5. Comparison of the B-mode ultrasound images for the MAMs and for the DiI dye flowing through the dialysis membrane tube: (1) before the therapeutic ultrasound pulses are applied, (2) during the application of the therapeutic ultrasound pulses, (3) immediately after the termination of the therapeutic ultrasound pulses. (A) and (B) correspond to the MAMs and the DiI dye respectively. The following operating parameters were used for therapeutic ultrasound probe: frequency 3 MHz, intensity 1 W/cm^2, duty cycle 20%, and duration 5 min.

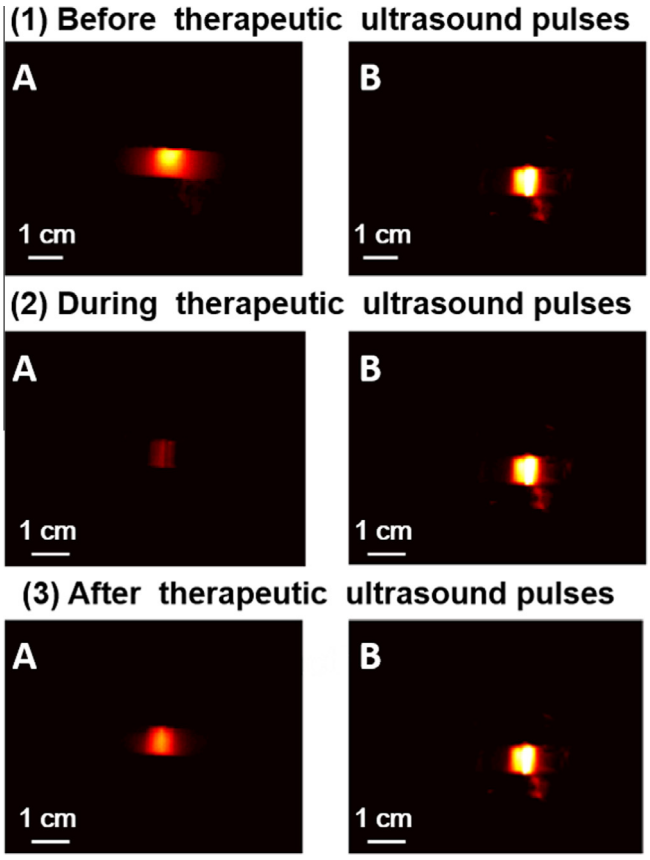

Fig. 6. Comparison of fluorescence images of the dialysis membrane tubes filled with the MAMs (A) and the DiI dye (B) respectively. The images were acquired before (1), during (2), and immediately after (3) the application of the therapeutic ultrasound pulses.

pulses, the vaporization of the MAMs disturbs the media and attenuates the fluorescence emission significantly, while no change of fluorescence emission is observed for the DiI dye (Fig. 6, 2A vs. 2B). After the termination of the ultrasound pulses, the fluorescence emission of the MAMs resumes to a lower level with a smaller boundary in comparison to the original status, whereas no change can be observed for the DiI dye (Fig. 6, 3A vs. 3B). The reduction of the fluorescence intensity for the MAMs may be explained by the release of the DiI dye to the solution and the formation of the large gas bubbles.

3.3. Ultrasound mediated release of oxygen from MAMs

Fig. 7 shows the oxygen partial pressure in the flow of MAMs before, during, and after the application of the therapeutic ultrasound pulses under the following test conditions: (a) the tube is filled with water at an oxygen partial pressure of 100 mm Hg (normoxia); (b) the tube is filled with normoxic water suspension of the oxygen-loaded MAMs; (c) the tube is filled with water at an oxygen partial pressure of 22 mm Hg (hypoxia); (d) the tube is filled with hypoxic water suspension of the oxygen-loaded MAMs. According to Figs. 7(a) and (c), applying therapeutic ultrasound pulses to water does not change its oxygen partial pressure significantly, no matter whether it is normoxic or hypoxic water. However, applying therapeutic ultrasound pulses to the oxygen loaded MAMs will release oxygen to the flow and introduce changes in oxygen partial pressure, as evidenced in Figs. 7(b) and (d). The level of oxygen partial pressure change depends on the test condition significantly. For hypoxic water suspension of the oxygen loaded MAMs, significant increase in oxygen partial pressure can be observed upon exposure to the therapeutic ultrasound pulses (Fig. 7(d)). In comparison, only slight increase in oxygen partial pressure can be observed for normoxic water suspension of the oxygen loaded MAMs after exposure to the therapeutic ultrasound pulses (Fig. 7(b)). These results imply that the MAMs are especially useful for delivering oxygen in a hypoxic environment.

3.4. Ultrasound mediated drug delivery in a porcine carotid artery model

Ultrasound mediated drug delivery was demonstrated in a porcine artery model using the DiI dye as a model drug. The freshly harvested porcine carotid artery was tied to the circulation system

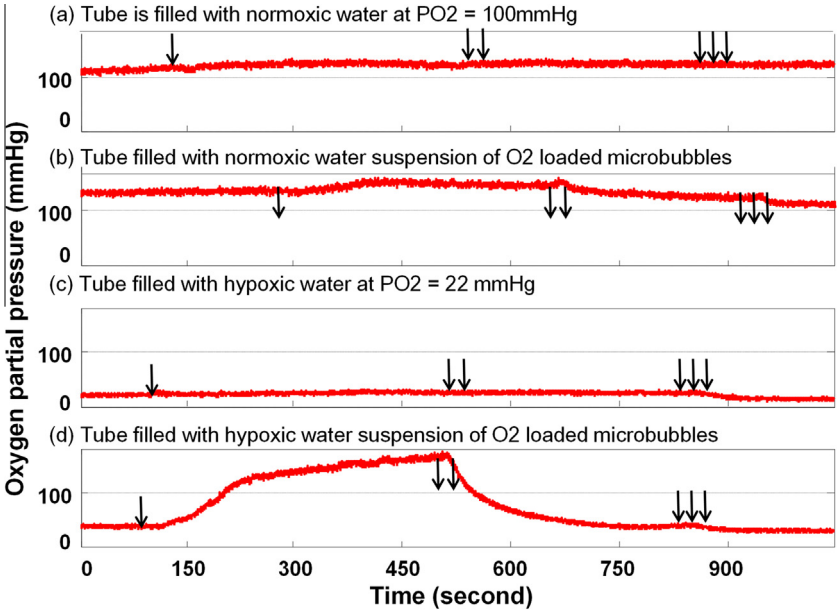

Fig. 7. Oxygen partial pressure of the flow circulated in the dialysis membrane tube before, during, and after the application of the therapeutic ultrasound pulses at four different test conditions. ↓: start applying therapeutic ultrasound pulses, ↓ ↓: stop applying therapeutic ultrasound pulses. ↓ ↓ ↓: stop flow circulation in the tube.

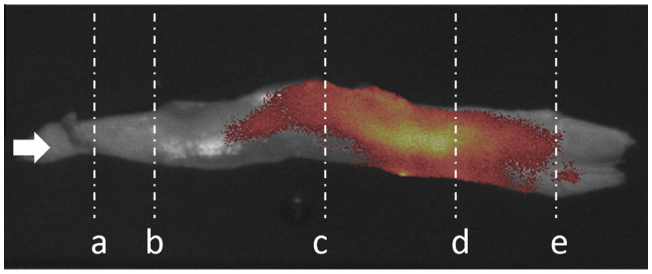

Fig. 8. Fusion of the background (gray scale) and the fluorescence (pseudo color) images of the bisected carotid artery after the application of the therapeutic ultrasound pulses. The white arrow indicates the flow direction. (a) is the location of the inlet connector where one end of the artery was tied to; (b) is the upstream of the MAM flow before the therapeutic ultrasound probe; (c) is location where the therapeutic ultrasound probe was placed; (d) is the downstream of the MAM flow after the exposure to ultrasound pulses; and (e) is the location of the outlet connector where the other end of the artery was tied to.

in Fig. 2 and the therapeutic ultrasound pulses were applied to the middle portion of the artery as the DiI loaded MAMs flowed through the vessel. The artery was bisected for fluorescence imaging after exposure to ultrasound pulses for 5 min. As shown in Fig. 8, no fluorescence emission can be observed at the inlet and the upstream locations of the flow of MAMs. However, at the location where the therapeutic ultrasound pulses were applied, the MAMs were activated and the DiI dye was released, leading to the significantly enhanced fluorescence intensity in the downstream of the flow of MAMs. Such a distribution pattern for fluorescence emission is reproducible in different tests, indicating the potential enhancement of drug delivery efficiency after MAM fragmentation.

The enhancement of drug delivery efficiency by ultrasound mediated MAM fragmentation is also confirmed by fluorescence microscopic imaging. Fig. 9 shows the fluorescence microscopic images of the frozen artery sections at five positions along the MAM flow direction (i.e., inlet, upstream, ultrasound pulse

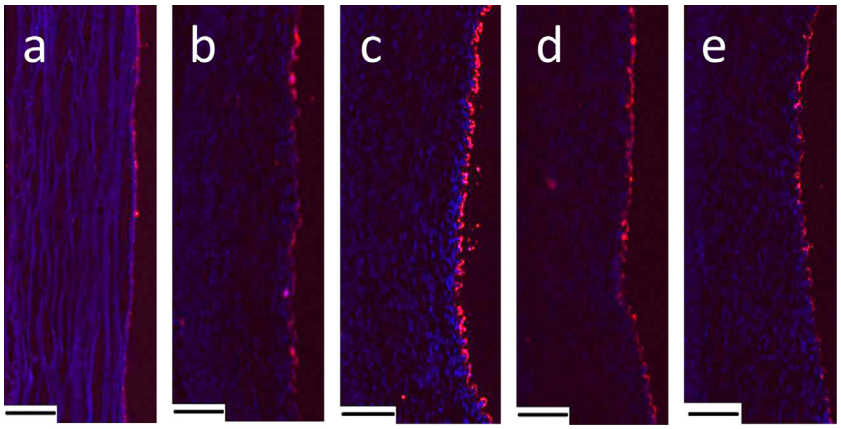

Fig. 9. Fluorescence microscopic images of the frozen tissue sections at five locations along the carotid artery (positions (a)–(e)). The frozen sections were stained with DAPI. The blue color shows the cells' nuclei. The pink color shows the deposition of the DiI dye. Scale bar = 200 μm. (For interpretation of the references to colour in this figure legend, the reader is referred to the web version of this article.)

activation, downstream, and outlet positions as marked in Fig. 8). By comparing the intensity of fluorescence emission from the DiI dye (marked in pink) at these positions, it can be observed that the DiI dye deposition is significantly enhanced upon exposure to ultrasound pulses.

4. Discussion

Owing to their superior chemical stability, biocompatibility, and unique physical characteristics, liquid PFC compounds have gained more and more clinical interests in recent years. PFC emulsions have been used as an artificial oxygen carrier since oxygen solubility in PFC is much greater than that in either water or blood and since oxygenated PFC maintains a high oxygen content for several days [21]. Some PFC compounds have relatively low boiling points and readily evaporate upon stimulation by external energy sources. They have been used to fabricate droplets, bubbles, or capsules at micro and nano sizes in various applications of image guided therapy and controlled drug delivery [22–26].

We integrated the oxygen loading and the vaporization capabilities of PFC compounds for simultaneous delivery of oxygen and drugs with imaging guidance by both ultrasound and fluorescence modalities. Oxygen and DiI loaded MAMs with an average size of 2.65 μm were fabricated by a modified emulsification process. The MAMs were circulated through either a dialysis membrane tube or a freshly harvested porcine carotid artery. The circulated MBs were activated by therapeutic ultrasound pulses at a frequency of 3 MHz, a power density of 1 W/cm^2, and a duty cycle of 20%. Ultrasound mediated fragmentation of the MAMs was monitored by a dissolved oxygen meter, a fluorescence imaging system, an ultrasound transducer, and a clinical ultrasound probe, respectively. Through a series of experiments, we demonstrated the following technical feasibilities for potential imaging and therapeutic applications.

First of all, therapeutic ultrasound pulses at a clinically safe dosage may stimulate the phase shift of PFC compounds for MAM fragmentation with increased echogenicity. This observation is coincident with previous reports [27,28], except that the MAMs in our study can be activated at a relatively lower acoustic power density. It is believed that the cavitation effect of the therapeutic ultrasound pulses and the PFC thermodynamic changes after dissolving oxygen may contribute to the reduced acoustic energy threshold for droplet-to-bubble transition. Further quantitative study is necessary in order to optimize the energy threshold for effective fragmentation of the MAMs with significant enhancement of acoustic contrast.

Second, therapeutic ultrasound pulses facilitate the release of oxygen from the MAMs to the surrounding hypoxic environment. Although gas-filled nanobubbles have been previously explored for ultrasound mediated delivery of oxygen [29], the mechanism behind the ultrasound mediated oxygen delivery from PFC droplets is more complicated. We believe that this mechanism is at least associated with the following four contributing factors. First of all, the ultrasound pulses introduce PFC phase shift that dramatically increases the interfacial surface area of a MAM, reduces its shell thickness, and facilitates the diffusion of oxygen to the surrounding environment. Second, the droplet-to-bubble transition and the rapid fragmentation of the MAMs further facilitate the release of oxygen [30]. Third, the mechanical perturbation and the sonication effect introduced by ultrasound pulses effective mix the solution for oxygen release. Finally, the oxygen gradient between the MAMs and the surrounding hypoxic environment further facilitates the effective oxygen transport. Considering that hypoxia is one of the most critical biologic disorders associated with many clinical anomalies, the oxygen-loaded MAMs may have a significant impact on the treatment of many life-threatening diseases in the future.

Third, ultrasound mediated fragmentation of the MAMs can be effectively monitored by both ultrasound and fluorescence imaging modalities. On the one hand, the increased echogenicity after acoustic droplet vaporization provides a superior contrast for ultrasound imaging. On the other hand, fragmentation of the fluorophore-loaded MAMs is accompanied with dramatic variations in fluorescence emission pattern that can be used for process monitoring. In our study, the DiI-loaded MAMs show a fluorescence emission boundary larger than that of the DiI dye, indicating the increased scattering coefficient and the enhanced migration of light. As the therapeutic ultrasound pulses are applied to the MAMs, the fluorescence emission is significantly diminished, possibly due to the formation of the light-blocking gas bubbles as the result of vaporization and cavitation. After ultrasound mediation, the fluorescence emission resumes to a certain extent, but cannot reach the same level as that before ultrasound mediation. The reduced fluorescent intensity may be associated with the different photon transport patterns for the DiI-loaded MBs before and after ultrasound mediation. Ultrasound mediation also breaks the highly-scattering MBs, reduces the scattering coefficient of the media, and results in a smaller but sharper fluorescence boundary, similar to that of the DiI dye. The acoustic and fluorescence variations during ultrasound mediated fragmentation of the MAMs may serve as a dynamic guidance for future drug delivery applications.

Finally, we have demonstrated the enhanced drug delivery efficiency after ultrasound mediated fragmentation of the drug-loaded MAMs in a porcine carotid artery model. Fluorescence imaging of the bisected carotid artery and confocal fluorescence imaging of the frozen tissue sections have confirmed the enhanced drug delivery efficiency, as coincident with the previous report [20]. Such enhanced drug delivery efficiency is associated with a series of complicated mechanisms involving both ultrasound mediated fragmentation of MBs and the biological effects of ultrasound [31]. Ultrasound pulses may introduce acoustic cavitation of MBs and enhance the transient cell membrane permeability for drug delivery [32]. Inertial cavitation of systemically injected MBs may damage the endothelial lining and temporarily increase vessel permeability [33]. In the absence of cavitation, acoustic streaming and radiation force may localize and concentrate droplets and bubbles near a vessel wall and assist the delivery of targeted agents [34]. For PFC nanoparticles with an outer lipid monolayer embedding lipophilic drugs, the drugs are released primarily through interactions between the lipid surface and the opposing targeted cell membrane, a process termed "contact facilitated lipid exchange" [26]. Due to the lack of high speed microscopic imaging tools, the DiI release pattern during the ultrasound mediated fragmentation of MAMs was not monitored continuously. Further study is necessary in order to understand this procedure for the optimal drug delivery outcome. The mechanism of ultrasound mediated droplet-to-bubble transition in PFC phase-shift nanoemulsions is not completely understood yet. The droplet-to-bubble transition is accompanied with a dramatic increased droplet volume and a reduced shell thickness. This is expected to favor the release of the encapsulated drugs, especially under the condition that the ultrasound pulses rip off the drugs from the bubble surface [31].

In summary, we have encapsulated oxygen enriched PFC compound in a lipid shell and loaded the DiI dye on the surface to test the hypothesis that ultrasound mediated fragmentation of the MAMs will facilitate controlled delivery of oxygen and therapeutics with improved efficiency. Our research demonstrated the technical potential of using MAMs for oxygen and drug delivery with ultrasound and fluorescence imaging guidance. To the best of the authors' knowledge, this research represents the first attempt for

simultaneous delivery of oxygen and drugs with both ultrasound and fluorescence imaging guidance.

5. Competing interests

The authors have declared that no competing interest exists.

Acknowledgements

The authors are grateful for the support of the following agencies: National Cancer Institute (R21CA15977), Natural Science Foundation of China (81372799, 81327803, 11472270), and Bureau Health Foundation of Chongqing (Project No. 2010-1-6). Experimental help from Jiwei Huang, Leilei Zhang, Dr.Wujie Zhang, Dr. Wei Rao, and Dr. Xiaoming He (all from Department of Biomedical Engineering of The Ohio State University) are greatly appreciated.

References

[1] R. Siegel, D. Naishadham, A. Jemal, Cancer statistics, 2013, CA Cancer J. Clin. 63 (2013) 11–30.
[2] R.C. Bast Jr., B. Hennessy, G.B. Mills, The biology of ovarian cancer: new opportunities for translation, Nat. Rev. Cancer 9 (2009) 415–428.
[3] R.M. Wenham, Ovarian cancer: a bright future, Cancer Control 18 (2011) 4–5.
[4] P. Vaupel, D.K. Kelleher, O. Thews, Modulation of tumor oxygenation, Int. J. Radiat. Oncol. Biol. Phys. 42 (1998) 843–848.
[5] J. Adamski, A. Price, C. Dive, G. Makin, Hypoxia-induced cytotoxic drug resistance in osteosarcoma is independent of HIF-1Alpha, PLoS ONE 8 (2013) e65304.
[6] L. Milane, S. Ganesh, S. Shah, Z.F. Duan, M. Amiji, Multi-modal strategies for overcoming tumor drug resistance: hypoxia, the Warburg effect, stem cells, and multifunctional nanotechnology, J. Control Release 155 (2011) 237–247.
[7] N. Rohwer, T. Cramer, Hypoxia-mediated drug resistance: novel insights on the functional interaction of HIFs and cell death pathways, Drug Resist. Updat. 14 (2011) 191–201.
[8] N.S. Al-Waili, G.J. Butler, J. Beale, R.W. Hamilton, B.Y. Lee, P. Lucas, Hyperbaric oxygen and malignancies: a potential role in radiotherapy, chemotherapy, tumor surgery and phototherapy, Med. Sci. Monit. 11 (2005) RA279–RA289.
[9] I. Moen, K.J. Tronstad, O. Kolmannskog, G.S. Salvesen, R.K. Reed, L.E. Stuhr, Hyperoxia increases the uptake of 5-fluorouracil in mammary tumors independently of changes in interstitial fluid pressure and tumor stroma, BMC Cancer 9 (2009) 446.
[10] J. Daruwalla, C. Christophi, Hyperbaric oxygen therapy for malignancy: a review, World J. Surg. 30 (2006) 2112–2131.
[11] F. Forsberg, D.A. Merton, J.B. Liu, L. Needleman, B.B. Goldberg, Clinical applications of ultrasound contrast agents, Ultrasonics 36 (1998) 695–701.
[12] F. Kiessling, J. Huppert, M. Palmowski, Functional and molecular ultrasound imaging: concepts and contrast agents, Curr. Med. Chem. 16 (2009) 627–642.
[13] K. Ferrara, R. Pollard, M. Borden, Ultrasound microbubble contrast agents: fundamentals and application to gene and drug delivery, Annu. Rev. Biomed. Eng. 9 (2007) 415–447.
[14] C. Pu, S. Chang, J. Sun, S. Zhu, H. Liu, Y. Zhu, Z. Wang, R.X. Xu, Ultrasound-mediated destruction of LHRHa-targeted and Paclitaxel-loaded lipid microbubbles for the treatment of intraperitoneal ovarian cancer xenografts, Mol. Pharm. 11 (2014) 49–58.
[15] H. Liu, S. Chang, J. Sun, S. Zhu, C. Pu, Y. Zhu, Z. Wang, R.X. Xu, Ultrasound-mediated destruction of LHRHa-targeted and paclitaxel-loaded lipid microbubbles induces proliferation inhibition and apoptosis in ovarian cancer cells, Mol. Pharm. 11 (2014) 40–48.
[16] L. Liu, S. Chang, J. Sun, S. Zhu, M. Yin, Y. Zhu, Z. Wang, R.X. Xu, Ultrasound-mediated destruction of paclitaxel and oxygen loaded lipid microbubbles for combination therapy in ovarian cancer xenografts, Cancer Lett. 361 (1) (2015) 147–154.
[17] Z. Zhu, T. Si, R.X. Xu, Microencapsulation of indocyanine green for potential applications in image-guided drug delivery, Lab Chip 15 (3) (2015) 646–649.
[18] R.X. Xu, J. Huang, J.S. Xu, D. Sun, G.H. Hinkle, E.W. Martin, S.P. Povoski, Fabrication of indocyanine green encapsulated biodegradable microbubbles for structural and functional imaging of cancer, J. Biomed. Opt. 14 (2009) 034020.
[19] J.S. Xu, J. Huang, R. Qin, G.H. Hinkle, S.P. Povoski, E.W. Martin, R.X. Xu, Synthesizing and binding dual-mode poly (lactic-co-glycolic acid) (PLGA) nanobubbles for cancer targeting and imaging, Biomaterials 31 (2010) 1716–1722.
[20] A.V. Patil, J.J. Rychak, A.L. Klibanov, J.A. Hossack, Real-time technique for improving molecular imaging and guiding drug delivery in large blood vessels: in vitro and ex vivo results, Mol. Imaging 10 (2011) 238–247.
[21] D.R. Spahn, R. Kocian, Artificial O2 carriers: status in 2005, Curr. Pharm. Des. 11 (2005) 4099–4114.
[22] J. Huang, J.S. Xu, R.X. Xu, Heat-sensitive microbubbles for intraoperative assessment of cancer ablation margins, Biomaterials 31 (2010) 1278–1286.
[23] R.X. Xu, S.P. Povoski, E.W. Martin Jr., Targeted delivery of microbubbles and nanobubbles for image-guided thermal ablation therapy of tumors, Expert Rev. Med. Devices 7 (2010) 303–306.
[24] N. Rapoport, K.H. Nam, R. Gupta, Z. Gao, P. Mohan, A. Payne, N. Todd, X. Liu, T. Kim, J. Shea, C. Scaife, D.L. Parker, E.K. Jeong, A.M. Kennedy, Ultrasound-mediated tumor imaging and nanotherapy using drug loaded, block copolymer stabilized perfluorocarbon nanoemulsions, J. Control Release 153 (2011) 4–15.
[25] J.R. Rajian, M.L. Fabiilli, J.B. Fowlkes, P.L. Carson, X. Wang, Drug delivery monitoring by photoacoustic tomography with an ICG encapsulated double emulsion, Opt. Express 19 (2011) 14335–14347.
[26] P.M. Winter, K. Cai, S.D. Caruthers, S.A. Wickline, G.M. Lanza, Emerging nanomedicine opportunities with perfluorocarbon nanoparticles, Expert Rev. Med. Devices 4 (2007) 137–145.
[27] O.D. Kripfgans, J.B. Fowlkes, D.L. Miller, O.P. Eldevik, P.L. Carson, Acoustic droplet vaporization for therapeutic and diagnostic applications, Ultrasound Med. Biol. 26 (2000) 1177–1189.
[28] K.-I. Kawabata, N. Sugita, H. Yoshikawa, T. Azuma, S.-I. Umemura, Nanoparticles with multiple perfluorocarbons for controllable ultrasonically induced phase shifting, Jpn. J. Appl. Phys. 44 (2005) 4548–4552.
[29] R. Cavalli, A. Bisazza, A. Rolfo, S. Balbis, D. Madonnaripa, I. Caniggia, C. Guiot, Ultrasound-mediated oxygen delivery from chitosan nanobubbles, Int. J. Pharm. 378 (2009) 215–217.
[30] G.L. Britton, H. Kim, P.H. Kee, J. Aronowski, C.K. Holland, D.D. McPherson, S.L. Huang, In vivo therapeutic gas delivery for neuroprotection with echogenic liposomes, Circulation 122 (2010) 1578–1587.
[31] B.E. O'Neill, N. Rapoport, Phase-shift, stimuli-responsive drug carriers for targeted delivery, Ther. Delivery 2 (2011) 1165–1187.
[32] A. van Wamel, K. Kooiman, M. Harteveld, M. Emmer, F.J. ten Cate, M. Versluis, N. de Jong, Vibrating microbubbles poking individual cells: drug transfer into cells via sonoporation, J. Control Release 112 (2006) 149–155.
[33] H. Chen, W. Kreider, A.A. Brayman, M.R. Bailey, T.J. Matula, Blood vessel deformations on microsecond time scales by ultrasonic cavitation, Phys. Rev. Lett. 106 (2011) 034301.
[34] P.A. Dayton, S. Zhao, S.H. Bloch, P. Schumann, K. Penrose, T.O. Matsunaga, R. Zutshi, A. Doinikov, K.W. Ferrara, Application of ultrasound to selectively localize nanodroplets for targeted imaging and therapy, Mol. Imaging 5 (2006) 160–174.